I&EC research
Industrial & Engineering Chemistry Research

pubs.acs.org/IECR

Article

Carbon Molecular Sieve Membranes with a Rationally Designed Polymer Precursor for Improved Propane/Propylene Separation

Published as part of the Industrial & Engineering Chemistry Research virtual special issue "Membranes for Sustainability".

Jiaqi Zhang, Zhenggong Wang,* and Jian Jin

Cite This: *Ind. Eng. Chem. Res.* 2023, 62, 18662−18671

Read Online

ACCESS | Metrics & More | Article Recommendations | Supporting Information

ABSTRACT: Membrane separation of propane and propylene provides a more energy-efficient route than traditional separation methods, such as distillation and absorption. Carbon molecular sieve (CMS) membranes with excellent chemical and physical stability have great potential in this separation process. The chemical structure of the polymer precursor greatly influences the separation performance of the CMS membrane. In this study, a benzimidazole-based polyimide is designed to manufacture CMS membranes for enhanced propane and propylene separation. The heterocyclic benzimidazole ring provides a flat chain structure to construct ultramicropores. Moreover, metal ions are homogeneously embedded in the polyimide precursor via a strong coordination interaction with the benzimidazole moiety. The microporous structure of the CMS membrane is further tailored owing to the steric hindrance of metal ions, which makes it difficult for larger C_3H_8 to penetrate. The pore structure changes in pristine CMS and metal ion modified CMS (M-CMS) are analyzed by wide-angle X-ray diffraction and gas adsorption measurement. The gas permeation data reveals that the M-CMS membrane demonstrates an improved C_3H_6/C_3H_8 selectivity (49.3) much higher than pristine CMS (18.6) and its comprehensive separation performance surpasses most of the reported CMS membranes for C_3H_6/C_3H_8 separation. This study demonstrates an effective strategy for preparing CMS membranes with tailored micropores for efficient propane/propylene separation.

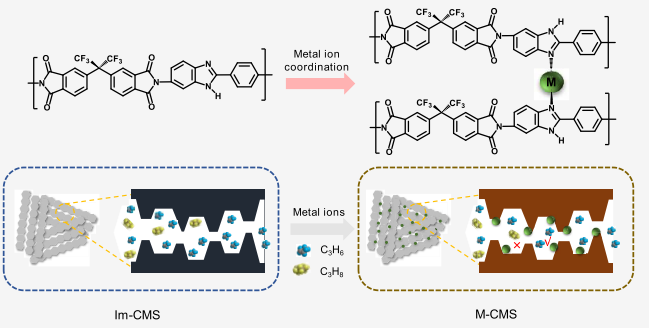

INTRODUCTION

C_3H_6 is an important chemical raw material used by the petrochemical industry to produce plastics and other fine chemicals.[1−3] C_3H_6 is mainly obtained by dehydrogenation of C_3H_8, so there is a large amount of C_3H_8 in the crude C_3H_6 product.[4,5] Currently, the separation of C_3H_6 and C_3H_8 in industry is mainly achieved through high-energy low-temperature distillation, which incurs high equipment investment and maintenance costs.[6−9] Membrane separation technology, as a highly efficient and energy-saving new separation technology, has great potential for application in the separation of C_3H_6 and C_3H_8.[10−12] However, the harsh operating conditions during C_3H_6/C_3H_8 separation combined with the low C_3H_6/C_3H_8 selectivity of current polymer membranes hinder the application of the polymer membrane in industrial production.[13,14]

Carbon molecular sieve (CMS) membranes have abundant micropores and ultramicropores due to the disordered stacking of carbon layers, which endow them with high gas permeability and selectivity.[15−18] Owing to their carbonaceous structure, CMS membranes possess better thermal and chemical stability over polymer membranes. Nevertheless, the formation process of an ideal CMS membrane is not easy, including complex cleavage and rearrangement reactions.[19] To date, there has been no systematic theoretical connection established between the performance of the precursor membrane and that of CMS membranes. However, many investigations indicate that the ultimate CMS performance is significantly influenced by the chemical and physical properties of polymer precursors.[20,21] Early CMS membranes used for C_3H_6/C_3H_8 separation mainly used commercial polyimide and phenolic resin as precursors.[22−24] These polymers usually have soft chain structures, and the resulting CMS membranes always have a low gas permeability. Matrimid as a commercial polyimide has been studied as a polymer precursor of CMS for C_3H_6/C_3H_8

Received: August 20, 2023
Revised: October 1, 2023
Accepted: October 11, 2023
Published: October 23, 2023

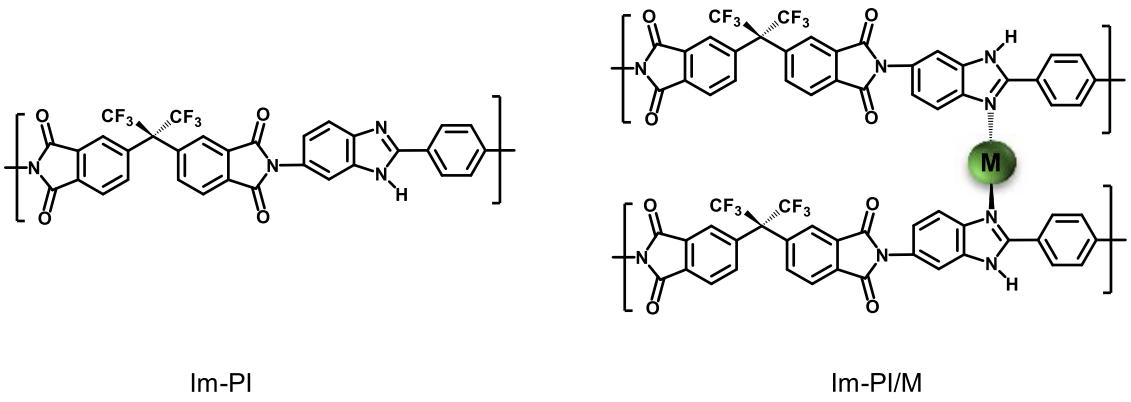

Figure 1. Chemical structure of benzimidazole polyimide and its metal ion complex.

separation. Steel et al. pyrolyzed a Matrimid precursor to prepare CMS membranes at different temperatures. A high pyrolysis temperature (800 °C) leads to both low permeability and gas selectivity.[25] A lower pyrolysis temperature of 500 °C brings more attractive separation performance of C_3H_6 permeability of 13 barrer and C_3H_6/C_3H_8 selectivity of 40. However, the low gas permeability could not meet high flux requirement in industrial production. Increasing the free volume of the polymer precursor has been proved an effective strategy to enhance permeability. Chung et al. prepared CMS using a polymer of intrinsic microporosity (PIM) copolymerized with cyclodextrin (CD) as a precursor in which the cyclodextrin structure formed abundant micropores after high-temperature removal.[26] Compared with PIM membranes without CD, C_3H_6 permeability of the partially carbonized PIM-CD membrane increased to 42 Barrer, while C_3H_6/C_3H_8 selectivity was only 8.4. To further increase the separation performance, Pinnau et al. used a hydroxyl-functionalized PIM-polyimide as a precursor to increase chain rigidity.[27] The resulting CMS membrane showed enhanced C_3H_6/C_3H_8 separation performance with higher C_3H_6 permeance (31 barrer) and C_3H_6/C_3H_8 selectivity (17). From the above discussion, it could be seen that the C_3H_6/C_3H_8 separation performance of the CMS membrane can be optimized by the rational precursor molecular structure design. However, the present precursor structures are quite limited[28−31] and there is still a lack of rationally designed precursor materials for constructing high-performance CMS membranes.

In this work, rationally designed polymer precursors are designed to prepare CMS membranes with improved propane/propylene separation. The pristine polyimide (Im-PI) is composed of a hexafluoroisopropyl and benzimidazole structure as shown in Figure 1. The rigid and twisted hexafluoroisopropyl structure hindered the molecular chain stacking and promoted abundant porous structure formation in the CMS membrane. The heterocyclic benzimidazole ring provides a flat chain structure to construct ultramicropores inside the resulting CMS. In addition, the benzimidazole units provide sufficient sites to the coordination interaction with transition-metal ions (Co^{2+} or Zn^{2+}). The coordination effect is beneficial for the uniform dispersion of metal ions in the CMS. After carbonization, metal ions are attached to the micropores and ultramicropores of the CMS membrane, blocking the ultramicropores to enhance the sieving effect on C_3H_6/C_3H_8. Compared with that of the pristine CMS membrane, the C_3H_6 and C_3H_8 selectivity of Co-CMS significantly increased from 18.6 to 49.3. The comprehensive separation performance of the Co-CMS membrane is superior to most reported CMS membranes. The work confirms the feasibility of our benzimidazole polyimide-derived CMS membrane in the application of C_3H_6/C_3H_8 separation.

EXPERIMENTAL SECTION

Materials. Anhydrous methanol and *N*,*N*-dimethylformamide (DMF) were purchased from Sinopharm Chemical Reagent Co., Ltd. Ultradry *N*-methyl 2-pyrrolidone (NMP) was purchased from Innochem. $CoCl_2$ and $Zn(NO_3)_2$ were supplied from Sigma-Aldrich. 2,2′-Bis(3,4′-dicarboxyphenyl) hexafluoropropane dianhydride (6FDA) and 2-(4-aminophenyl)-1*H*-benzimidazol-5-amine (PABZ) were purchased from TCI chemicals (China) and dried under reduced pressure for 12 h before used.

Synthesis of Polymer Precursors. Im-PI was synthesized via a polycondensation reaction between dianhydride and diamine monomer as reported in our previous work.[32] Specifically, PABZ (2.24 g, 0.01 mol) was dissolved in ultradry NMP (100 mL) in a 250 mL three-neck flask. After the solid was completely dissolved, 6FDA (4.44 g, 0.01 mol) was added in portions to the flask equipped with a Dean−Stark trap and reflux condenser. The mixture was stirred at room temperature for 12 h under a nitrogen atmosphere. Then, the reaction temperature was gradually increased to 200 °C and held for another 6 h. Afterward, the viscous solution was poured slowly into 600 mL of anhydrous methanol. The resulting solid precipitate was soaked in anhydrous methanol to remove the residual organic solvent, and the methanol solution was replaced every 12 h. Finally, the product was placed in a vacuum oven and dried at 120 °C for 12 h, giving Im-PI as a light-yellow thread-like solid.

Fabrication of CMS Membranes. The precursor membranes were prepared by using the solution casting method. 0.3 g of Im-PI was dissolved in DMF to form a homogeneous 3 wt % solution. After being stirred for 12 h, the solution was filtered with a 0.45 μm PTFE syringe filter. Then, a certain amount of salt DMF solution ($CoCl_2$ or $Zn(NO_3)_2$) was dropped into the polymer solution and stirred for 2 h. The mixed solution was allowed to stand for 30 min to remove air bubbles and then poured into a 9 cm diameter glass dish. The membrane was obtained by slow solvent evaporation for 24 h in a drying oven at 60 °C. Then, the obtained membrane was placed in a high-vacuum, oil-free oven at 120 °C for 24 h to remove the residual solvent.

For the preparation of CMS membranes, a precursor membrane with a diameter of 2 cm was sandwiched between

https://doi.org/10.1021/acs.iecr.3c02933
Ind. Eng. Chem. Res. 2023, 62, 18662−18671

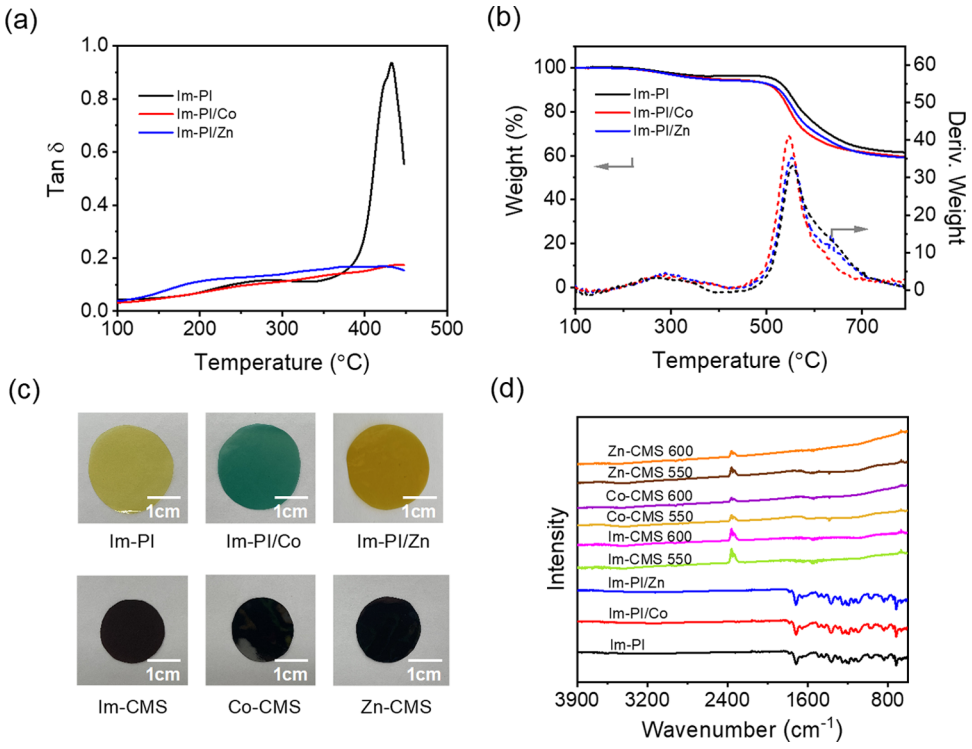

Figure 2. (a) DMA curves; (b) TGA and differential thermogravimetric curves of Im-PI, Im-PI/Co, and Im-PI/Zn membranes; (c) Optical photographs; and (d) FTIR spectra of Im-PI, Im-PI/M, and their CMS membranes.

two quartz plates and then placed in a tubular furnace. The quartz tube was purged with ultrahigh-purity argon for 1 h, and the membrane was pyrolyzed under the condition of flowing argon (200 cc/min). The pyrolysis schemes of CMS membranes at different temperatures are shown in Figure S1. The CMS membranes derived from Im-PI and its metal complex precursor are named after Im-CMS and M-CMS, respectively.

Characterization. Thermogravimetric analysis (TGA) was performed on a TG/DTA 6200 (Seiko Instruments, Inc.) instrument to characterize the weight loss and thermal stability of the polymer precursor during the pyrolysis process. Dynamic mechanical property of the precursor was confirmed by a DMA Q800 analyzer, with a load frequency of 1 Hz and a heating rate of 3 °C/min, from 25 to 450 °C under a nitrogen atmosphere. Fourier transform infrared (FTIR) spectra were used to determine the functional groups in membranes on Nicolet 6700 spectroscopy. Raman spectra were obtained from a Horiba LabRAM ARAMIS Raman microscope using 473 nm laser irradiation. Wide-angle X-ray diffraction (WAXD) patterns were collected on a Bruke D8 instrument equipped with Cu Kα radiation of wavelength (λ) 1.54 Å over a scanning range of 5−40°. CO_2, C_3H_6, and C_3H_8 adsorption experiments were conducted on a Quantachrome Autosorb IQ-MP-MP at 273 K. The apparent surface areas were calculated by a multipoint Brunauer−Emmet−Teller (BET) method from CO_2 adsorption data, and the pore size distribution was calculated by a density functional theory (DFT) model.

RESULTS AND DISCUSSION

Characterization of the Polymer Precursor and CMS Membranes. The glass transition temperatures (T_g) of Im-PI and Im-PI/M membranes were characterized by dynamic thermomechanical analysis (DMA), as shown in Figure 2a. The T_g of the Im-PI polymer is as high as 430 °C, while T_g of most polyimides reported in the literature is approximately 300−400 °C.[33] This is due to the strong interchain interactions, including the $\pi-\pi$ interaction and hydrogen bonding between the chain segments of benzimidazole. The T_g of Im-PI/Co and Im-PI/Zn membranes is further increased above 450 °C. The results indicate that the chain segment mobility of Im-PI/M is confined due to the coordination bonds in the interchain. Thermogravimetric analysis (TGA) measurements were performed on Im-PI and Im-PI/M membranes to determine the pyrolysis temperature for preparing the CMS membrane. Figure 2b shows the TGA curves and the corresponding derivative thermogravimetry (DTG) curves of Im-PI and Im-PI/M membranes. According to the thermogravimetric differential curves, Im-PI and Im-PI/M membranes were carbonatized in the range of 500−650 °C to investigate the physical properties, chemical composition, and separation performance. In this temperature range, the polymer degrades violently and can provide abundant micropores and ultramicropores without overdensification, resulting in decreased gas permeability.

The CMS membranes of both Im-PI and Im-PI/M are prepared at elevated temperatures in an inert gas atmosphere. The detailed pyrolysis protocols are shown in Figure S2. The optical photographs of the precursor and CMS membranes are shown in Figure 2c. After heat treatment, the color of the membranes changed from clear and transparent to opaque dark black. The chemical structures of Im-PI and Im-PI/M before and after carbonization were characterized by ATR-FTIR as shown in Figure 2d. The typical characteristic peaks at 1780, 1720, 1368, and 720 cm^{-1} of polyimides can be seen in the infrared spectra of Im-PI, Im-PI/Co, and Im-PI/Zn membranes. After carbonization, the above characteristic peaks disappear in the infrared spectra of the carbon

https://doi.org/10.1021/acs.iecr.3c02933
Ind. Eng. Chem. Res. 2023, 62, 18662−18671

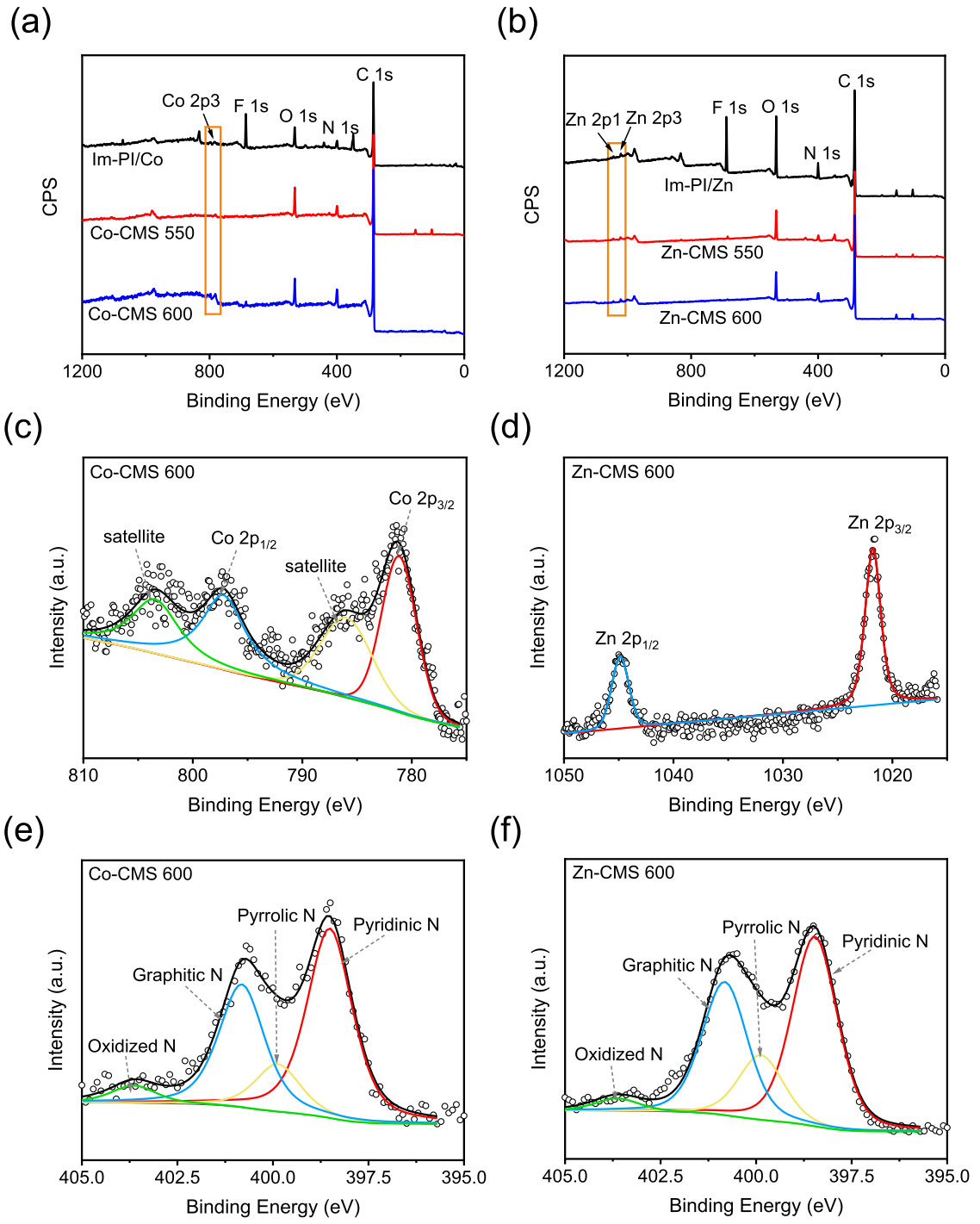

Figure 3. XPS spectra of Im-PI/M and CMS membranes: (a) Im-PI/Co and Co-CMS membranes; (b) Im-PI/Zn and Zn-CMS membranes; (c) Co 2p; (d) Zn 2p; and (e–f) N 1s.

membrane, indicating that the membrane changes from an organic polymer membrane to an inorganic carbon membrane.

Furthermore, Im-PI/M and their CMS membranes (Co-CMS and Zn-CMS) were analyzed by wide-scan X-ray photoelectron spectroscopy (XPS). As Figure 3a,b shows, the F 1s spectra almost disappeared after carbonization because the $-CF_3$ functional group of the 6FDA unit would be decomposed at approximately 500 °C. In addition, the spectra of Co 2p and Zn 2p were also detected in Co-CMS and Zn-CMS membranes, which proved that the CMS was successfully doped with metal ions. Figure 3c,d shows the Co 2p and Zn 2p spectra of Co-CMS 600 and Zn-CMS 600 membranes. The binding energy at 781.1 eV is Co $2p_{3/2}$, accompanied by satellite peaks. The binding energies at 1021.7 and 1044.8 eV can be attributed to Zn $2p_{3/2}$ and Zn $2p_{1/2}$. Figure 3e,f shows the high-resolution N 1s spectra of Co-CMS 600 and Zn-CMS 600 membranes, respectively. Four kinds of nitrogen can be obtained by peak fitting: pyridine nitrogen (398.5 eV), pyrrole nitrogen (399.9 eV), graphite nitrogen (400.8 eV), and nitrogen oxide (403.7 eV). The content of pyridine nitrogen is much greater than that of pyrrole nitrogen, and pyridine nitrogen can coordinate with Co^{2+} and Zn^{2+}. The above results

https://doi.org/10.1021/acs.iecr.3c02933
Ind. Eng. Chem. Res. 2023, 62, 18662−18671

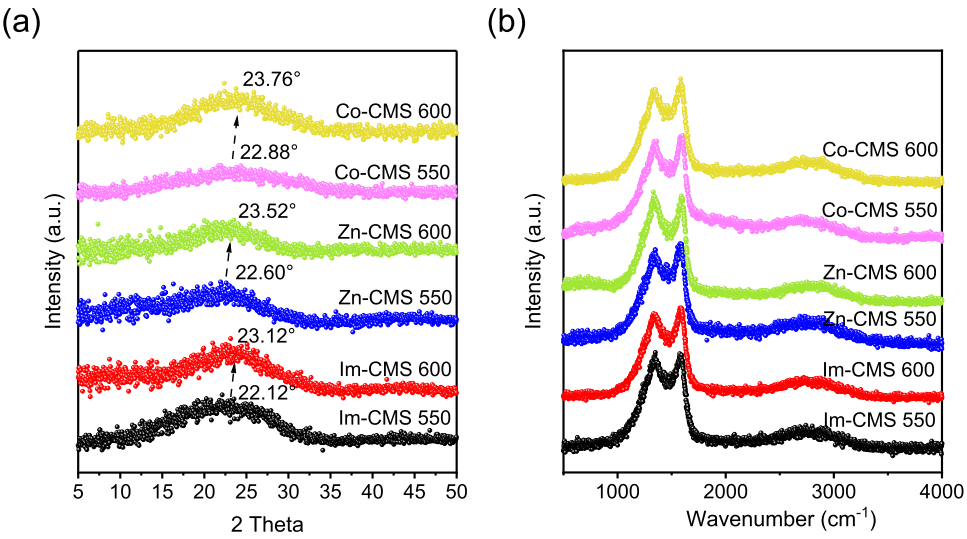

Figure 4. (a) Wide-angle X-ray diffraction and (b) Raman spectra of Im-CMS and M-CMS membranes.

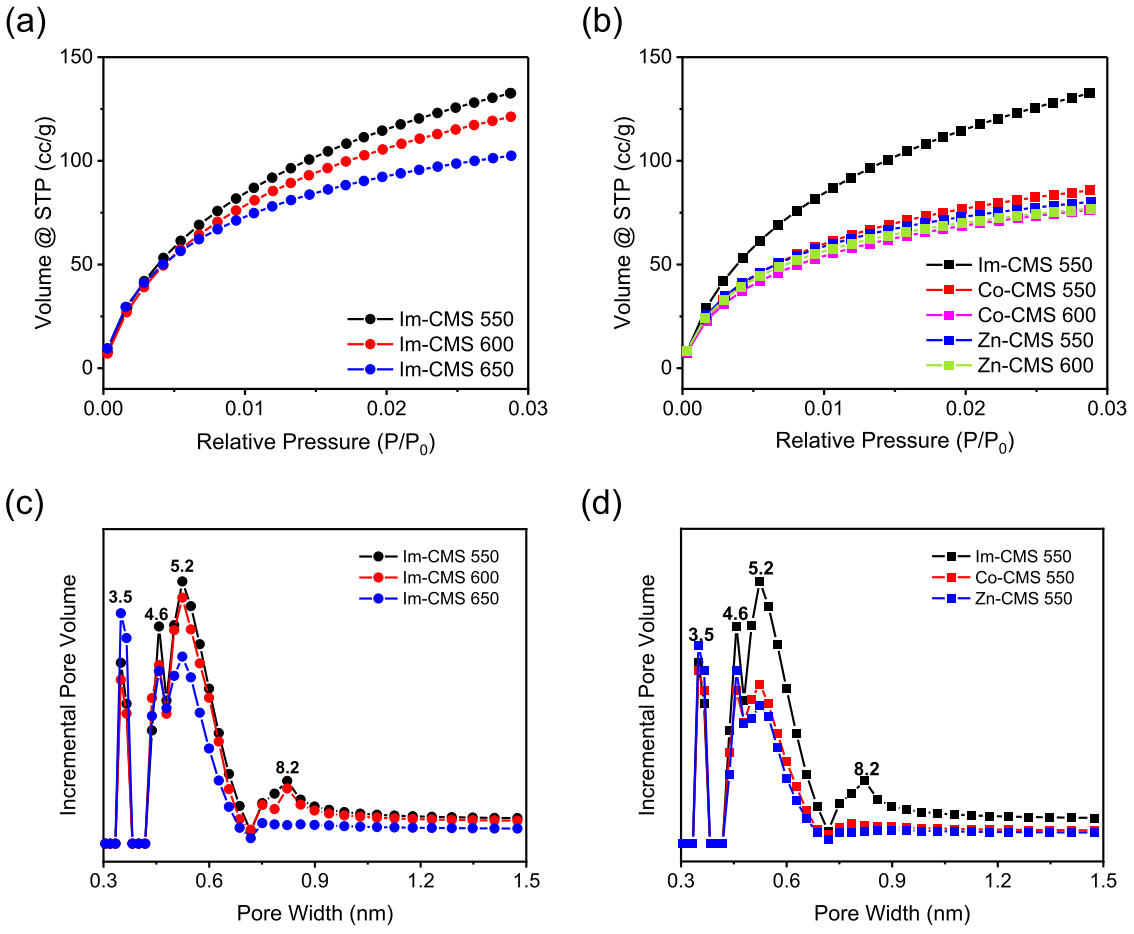

Figure 5. (a, b) CO_2 adsorption isotherms of Im-CMS and M-CMS membranes measured at 273 K and (c, d) pore size distributions of the membranes obtained from CO_2 adsorption measurements.

indicate that Co and Zn in CMS mainly exist in the form of Co^{2+} and Zn^{2+}, and they form complexes with pyridine nitrogen in CMS.

The microstructures of Im-CMS, Co-CMS, and Zn-CMS membranes carbonized at 550 and 600 °C were investigated by WAXD (Figure 4a). The WAXD spectra of all CMS membranes have a wide peak between 20 and 30°, showing the amorphous carbon structure. As the pyrolysis temperature increased from 550 to 600 °C, the peaks of all CMS membranes shifted to the right to varying degrees. The peak position of Im-CMS was increased from 22.04 to 23.12° (corresponding to the *d*-spacing decreasing from 4.02 to 3.85 Å). This indicates that the higher the pyrolysis temperature, the denser the structure of the carbon membrane. In addition,

https://doi.org/10.1021/acs.iecr.3c02933
Ind. Eng. Chem. Res. 2023, 62, 18662−18671

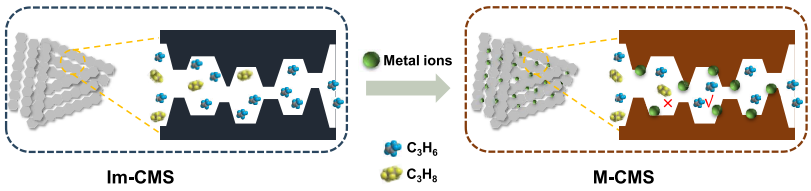

Figure 6. Schematic diagram of micropore and ultramicropore in Im-CMS and M-CMS membranes.

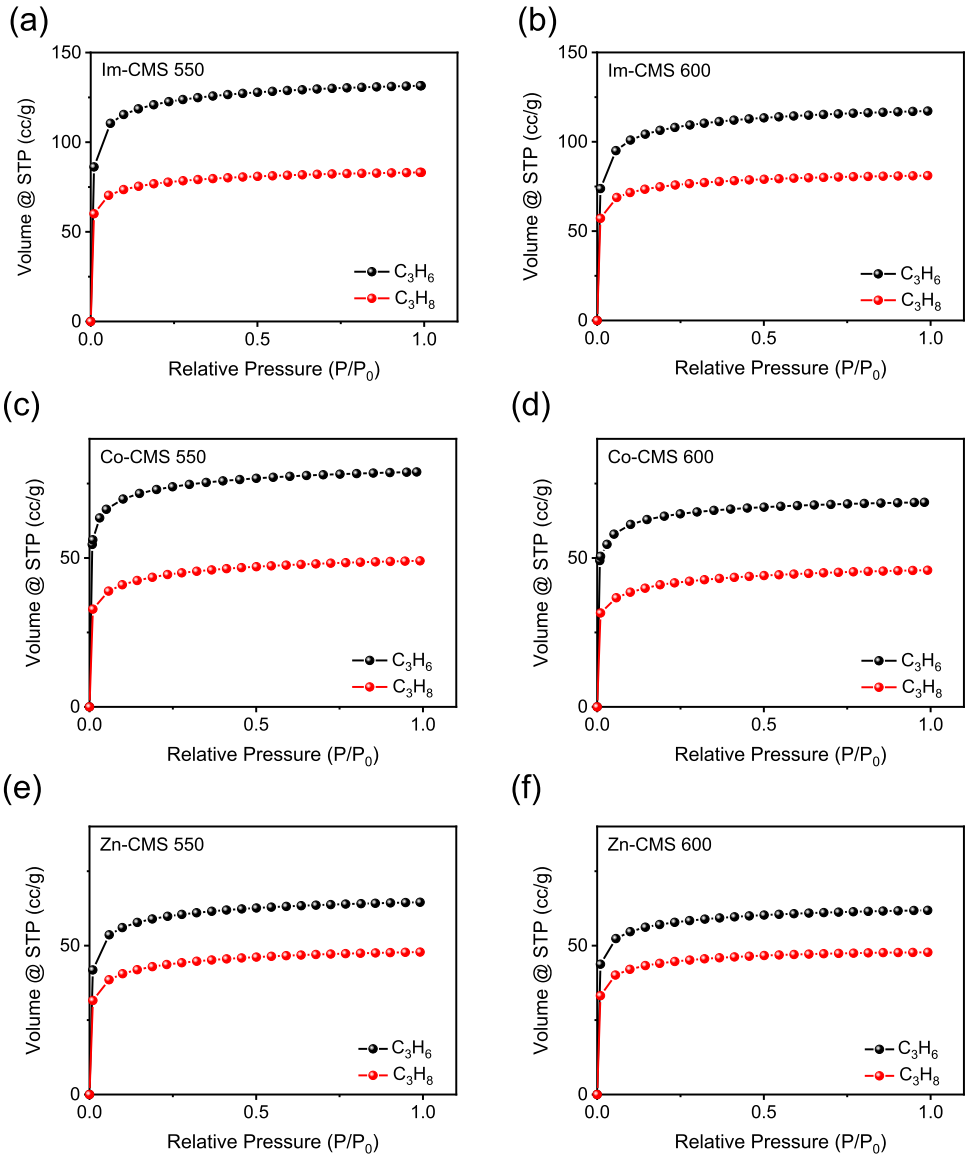

Figure 7. Adsorption isotherms of C_3H_6 and C_3H_8 at 273 K. (a) Im-CMS 550 membrane; (b) Im-CMS 600 membrane; (c) Co-CMS 550 membrane; (d) Co-CMS 600 membrane; (e) Zn-CMS 550 membrane; and (f) Zn-CMS 600 membrane.

M-CMS membranes had a smaller carbon layer spacing than the Im-CMS carbon membrane. The interlayer spacings of Co-CMS 600 and Zn-CMS 600 are 3.74 and 3.78 Å, respectively, which are smaller than that of Im-CMS 600 (3.85 Å). Raman spectroscopy was used to further analyze the carbon structure of the carbon membrane, as shown in Figure 4b. The Raman spectra of all CMS membranes show two peaks at 1580 and 1350 cm^{-1}, corresponding to disordered carbon (D band) and graphitic carbon (G band). This result shows that the carbon membrane has a short-range ordered and long-range disordered carbon structure.

The microporous structures of Im-CMS and M-CMS membranes are further characterized by gas adsorption tests. The CO_2 adsorption isotherms of Im-CMS, Co-CMS, and Zn-CMS CMS membranes at 273 K are shown in Figure 5a,b. Pore structure parameters calculated from the adsorption isotherm are summarized in Table S1. With increasing pyrolysis temperature, the CO_2 adsorption capacity of CMS membranes decreased gradually (132.6 cm^3/g for the Im-CMS 550 carbon membrane, 121.2 cm^3/g for the Im-CMS 600 carbon membrane, and 102.4 cm^3/g for the Im-CMS 650 carbon membrane). In addition, M-CMS membranes have a

https://doi.org/10.1021/acs.iecr.3c02933
Ind. Eng. Chem. Res. 2023, 62, 18662−18671

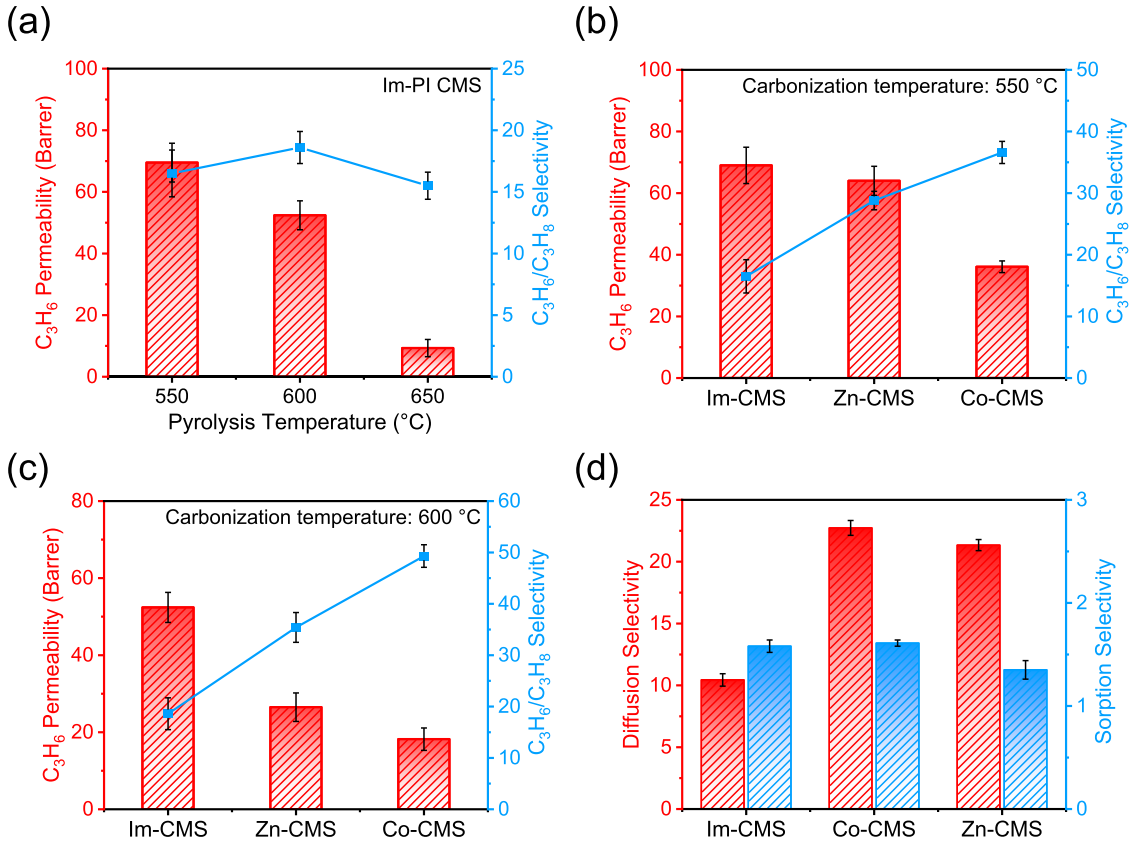

Figure 8. (a) Relationship between pyrolysis temperature and the C_3H_6/C_3H_8 separation performance of Im-CMS membranes; (b) C_3H_6/C_3H_8 separation performance of CMS membranes at 550 °C before and after doping metal ions; (c) C_3H_6/C_3H_8 separation performance of CMS membranes at 600 °C before and after doping metal ions; and (d) diffusion and sorption selectivity of C_3H_6 and C_3H_8 for CMS membranes at 550 °C before and after doping metal ions.

lower CO_2 adsorption capacity than Im-CMS membranes. The CO_2 adsorption capacities of Co-CMS 550 and Zn-CMS 550 membranes are 84.6 and 79.3 cm^3/g, which are 36.2 and 40.2% lower than that of the Im-CMS 550 carbon membrane, respectively. The B.E.T. specific surface area calculated from the CO_2 adsorption isotherm of the carbon membrane also decreases with increasing pyrolysis temperature and the addition of metal ions. Figure 5c shows the pore size distribution of Im-CMS membranes with different pyrolysis temperatures, which is calculated by nonlocalized density functional theory (NLDFT) from the CO_2 adsorption isotherm. As the pyrolysis temperature increased from 550 to 650 °C, the intensity related to micropores at 4−7 Å decreased significantly while that at 3−4 Å increased slightly, and the average pore size decreased. Figure 5d shows the pore size distributions of Im-CMS and M-CMS membranes. Doping metal has a similar effect with increasing carbonization temperature, reducing the average pore size of CMS membranes from 5.2 to 4.6 Å. This result further indicates that the doping of metal ions could finely tune the pore size of the CMS membrane, as illustrated in Figure 6.

The adsorption isotherms of C_3H_6 and C_3H_8 for different CMS membranes are shown in Figure 7, and the adsorption data are summarized in Table S1. The adsorption capacity of C_3H_6 and C_3H_8 decreases with an increasing pyrolysis temperature. The adsorption capacities of C_3H_6 and C_3H_8 of the Im-CMS 550 membrane are 131.5 and 83.2 cm^3/g, and those of the Im-CMS 600 membrane are 117.2 and 81.1 cm^3/g. However, the adsorption capacities of C_3H_6 and C_3H_8 of the Im-CMS 650 membrane decreased to 80.2 and 63.3 cm^3/g. In addition, the adsorption capacities of C_3H_6 and C_3H_8 of Co-CMS and Zn-CMS membranes also decreased. The C_3H_6 and C_3H_8 adsorption capacities of the Co-CMS 550 carbon membrane are 78.9 and 49 cm^3/g, while those of the Zn-CMS 550 carbon membrane are 64.5 and 47.8 cm^3/g. When the pyrolysis temperature is increased to 600 °C, the C_3H_6 and C_3H_8 adsorption capacities of Co-CMS 600 and Zn-CMS 600 membranes decrease to 68.7, 45.9, and 61.8, 47.7 cm^3/g, respectively. This may be because doped metal ions reduce the pore size of the CMS membrane.

Gas Separation Performance of CMS Membranes. The C_3H_6 and C_3H_8 gases permeation tests of CMS membranes were performed on a fixed-volume pressure increase time-lag apparatus with 3 bar feed gas at 35 °C. The gas permeability and C_3H_6/C_3H_8 selectivity are summarized in Figure 8a−c. The C_3H_6/C_3H_8 separation performance of Im-CMS membranes prepared at different temperatures is shown in Figure 8a. The C_3H_6 permeability and C_3H_6/C_3H_8 selectivity of the Im-CMS 550 carbon membrane were 69.5 Barrer and 16.5. By increasing the pyrolysis temperature from 550 to 600 °C, the C_3H_6 permeability of the Im-CMS 600 carbon membrane decreased slightly to 52.4 Barrer, while the C_3H_6/C_3H_8 selectivity increased to 18.6. As the pyrolysis temperature increases to 650 °C, the separation performance of C_3H_6/C_3H_8 decreases significantly with the permeability of C_3H_6 decreasing to 9.3 Barrer and the selectivity of C_3H_6/C_3H_8 decreasing to 15.5. The results indicate that the pyrolysis temperature has a

https://doi.org/10.1021/acs.iecr.3c02933
Ind. Eng. Chem. Res. 2023, 62, 18662−18671

significant effect on the C_3H_6/C_3H_8 separation performance of the CMS membranes. A controlled pyrolysis temperature can shrink the pore structure to hinder the transmission of C_3H_8 with a large kinetic diameter. When the pyrolysis temperature is too high, it is difficult for both C_3H_6 and C_3H_8 to pass through the pore, resulting in a decrease of both permeability and selectivity. Based on the above discussion, we chose M-CMS membranes obtained at 550 and 600 °C to further investigate the effect of metal ions doping on the C_3H_6/C_3H_8 separation performance. Figure 8b,c compares the C_3H_6/C_3H_8 separation performance of Im-CMS and M-CMS membranes with the same pyrolysis temperature. The C_3H_6/C_3H_8 selectivities of Zn-CMS 550 and Co-CMS 550 membranes are 28.8 and 36.6, while that of the Im-CMS 550 membrane is only 16.5. In addition, the C_3H_6/C_3H_8 selectivity of the Co-CMS 600 membrane is as high as 49.3, while that of the Im-CMS 600 membrane is only 18.6. It can be found that doping metal ions effectively improves the C_3H_6/C_3H_8 selectivity of CMS membranes.

To investigate the gas transportation mechanism in Im-CMS and M-CMS membranes, the solubility and diffusion coefficients of C_3H_6 and C_3H_8, as well as the solubility and diffusivity selectivity of C_3H_6/C_3H_8 are calculated based on the adsorption and permeation data. As shown in Figure 8d, increasing the pyrolysis temperature and doping metal ions had no significant effect on the sorption selectivity of C_3H_6/C_3H_8 CMS membranes, which is always approximately 1.3−1.5. However, the C_3H_6/C_3H_8 diffusion selectivity of Im-CMS membranes is effectively improved by increasing the pyrolysis temperature. As the pyrolysis temperature increased from 550 to 600 °C, the C_3H_6/C_3H_8 diffusion selectivity of Im-CMS membranes increased from 10.4 to 12.8 with an increase of 22.9%. The C_3H_6/C_3H_8 diffusion selectivity of the M-CMS membranes is greatly improved. The diffusion selectivity of the Im-CMS 550 membrane is 10.4, while those of Co-CMS 550 and Zn-CMS 550 membranes are 22.7 (117.6%) and 27.3 (161.7%). This is because doped metal ions lead to a decrease in the pore size of the CMS membrane, which hinders the transportation of larger C_3H_8 molecules, thus improving the diffusion selectivity. To evaluate the comprehensive separation performance of our CMS membranes, we compared the C_3H_6 permeability and C_3H_6/C_3H_8 selectivity of Im-CMS and M-CMS with the upper bound.[34] As shown in Figure 9 and Table S2, the C_3H_6/C_3H_8 separation performances of Im-CMS, Co-CMS, and Zn-CMS membranes prepared in this work far exceeded the upper bound, and the C_3H_6/C_3H_8 selectivity was higher than that of most reported membranes.[25−28,35−39] The exceptional separation performance of our CMS membrane makes it highly promising for the separation of olefins and paraffins.

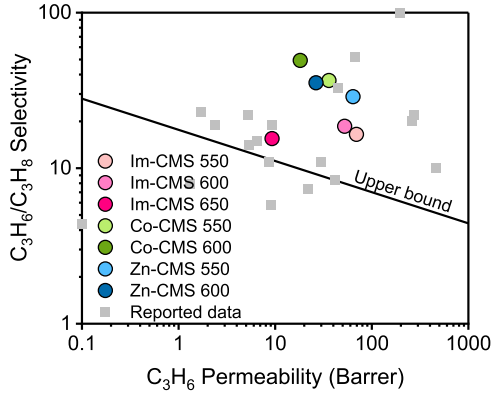

Figure 9. Upper bound plot of C_3H_6/C_3H_8 selectivity versus C_3H_6 permeability of our CMS and reported CMS membranes.

CONCLUSIONS

In this study, we used benzimidazole polyimide (Im-PI) and its metal complexes as precursors to prepare carbon molecular sieve membranes for C_3H_6/C_3H_8 separation by pyrolysis at different temperatures. The rationally designed structure of the precursor plays a crucial role in determining the pore structure of the resulting CMS membrane. The specific pore sizes and distributions are finely controlled in the resulting CMS membranes, which are well-characterized by WAXD and gas adsorption measurements. The C_3H_6/C_3H_8 selectivities of the Im-CMS membrane obtained at 550 and 600 °C are 16.5 and 18.6. After the doping of Co^{2+} and Zn^{2+} into the Im-PI precursor, the C_3H_6/C_3H_8 separation performance of the M-CMS membrane is further enhanced. The C_3H_6/C_3H_8 selectivities of Co-CMS membranes obtained at 550 and 600 °C are 36.6 and 49.3, respectively. This could be attributed to the steric hindrance of metal ions inside the micropore, leading to the large enhancement of C_3H_6/C_3H_8 diffusion selectivity. Our CMS membranes, which have been designed with a rationally designed precursor, exhibit exceptional separation performance for C_3H_6/C_3H_8 compared to the majority of reported CMS membranes. This finding offers valuable insights into the design of polymer precursors for the development of high-performance CMS membranes.

ASSOCIATED CONTENT

Supporting Information

The Supporting Information is available free of charge at https://pubs.acs.org/doi/10.1021/acs.iecr.3c02933.

Gas permeation measurements; *d*-spacing characterization; heating procedure of the carbonization process; flowchart of the preparation of the CMS membrane; gas adsorption data; and C_3H_6/C_3H_8 separation performance of the reported CMS membranes (PDF)

AUTHOR INFORMATION

Corresponding Author

Zhenggong Wang − *College of Chemistry, Chemical Engineering and Materials Science, Jiangsu Key Laboratory of Advanced Functional Polymer Design and Application, Collaborative Innovation Center of Suzhou Nano Science and Technology, Jiangsu Key Laboratory of Advanced Negative Carbon Technologies, Soochow University, Suzhou 215123, China; Xinjiang Zhongtai Chemical Co., Ltd., Urumqi 830000, China;* orcid.org/0000-0003-1671-1803; Email: zgwang2017@suda.edu.cn

Authors

Jiaqi Zhang − *College of Chemistry, Chemical Engineering and Materials Science, Jiangsu Key Laboratory of Advanced Functional Polymer Design and Application, Collaborative Innovation Center of Suzhou Nano Science and Technology, Jiangsu Key Laboratory of Advanced Negative Carbon Technologies, Soochow University, Suzhou 215123, China*

Jian Jin − *College of Chemistry, Chemical Engineering and Materials Science, Jiangsu Key Laboratory of Advanced*

Functional Polymer Design and Application, Collaborative Innovation Center of Suzhou Nano Science and Technology, Jiangsu Key Laboratory of Advanced Negative Carbon Technologies, Soochow University, Suzhou 215123, China; orcid.org/0000-0003-0429-300X

Complete contact information is available at: https://pubs.acs.org/10.1021/acs.iecr.3c02933

Author Contributions

Initial idea and experimental design: Z.G.W.; experiment and characterization: J.Q.Z.; analysis and comments: all authors; supervision: Z.G.W. and J.J.; writing—original draft: J.Q.Z. and Z.G.W.; writing—review and editing: J.Q.Z., Z.G.W., and J.J.

Notes

The authors declare no competing financial interest.

■ ACKNOWLEDGMENTS

This work was supported by the National Natural Science Foundation of China (22378282, 21988102, 51873230), the Natural Science Foundation of the Jiangsu Higher Education Institutions of China (23KJB150029), and the Key Development Project of Jiangsu Province (BE2022056).

■ REFERENCES

(1) Luo, Z.; Zheng, T.; Li, H.; Zhou, Q.; Wang, A.; Zhang, L.; Hu, Y. A submicron spherical polypropylene prepared by heterogeneous ziegler-natta catalyst. *Ind. Eng. Chem. Res.* **2015**, *54* (44), 11247−11250.

(2) Kaminsky, W. Highly active metallocene catalysts for olefin polymerization. *J. Chem. Soc., Dalton Trans.* **1998**, No. 9, 1413−1418, DOI: 10.1039/a800056e.

(3) Zhu, J.; Yuan, S.; Wang, J.; Zhang, Y.; Tian, M.; Van der Bruggen, B. Microporous organic polymer-based membranes for ultrafast molecular separations. *Prog. Polym. Sci.* **2020**, *110*, No. 101308.

(4) Pellis, A.; Malinconico, M.; Guarneri, A.; Gardossi, L. Renewable polymers and plastics: Performance beyond the green. *New Biotechnol.* **2021**, *60*, 146−158.

(5) Xiang, D.; Yang, S.; Liu, X.; Mai, Z.; Qian, Y. Techno-economic performance of the coal-to-olefins process with CCS. *Chem. Eng. J.* **2014**, *240*, 45−54.

(6) Kroon, M. C.; Vega, L. F. Selective paraffin removal from ethane/ethylene mixtures by adsorption into aluminum methylphosphonate-alpha: A molecular simulation study. *Langmuir* **2009**, *25* (4), 2148−2152.

(7) Amedi, H. R.; Aghajani, M. Economic estimation of various membranes and distillation for propylene and propane separation. *Ind. Eng. Chem. Res.* **2018**, *57* (12), 4366−4376.

(8) Faiz, R.; Li, K. Olefin/paraffin separation using membrane based facilitated transport/chemical absorption techniques. *Chem. Eng. Sci.* **2012**, *73*, 261−284.

(9) Wang, X.; Wu, Y.; Zhou, X.; Xiao, J.; Xia, Q.; Wang, H.; Li, Z. Novel C-PDA adsorbents with high uptake and preferential adsorption of ethane over ethylene. *Chem. Eng. Sci.* **2016**, *155*, 338−347.

(10) Faiz, R.; Li, K. Polymeric membranes for light olefin/paraffin separation. *Desalination* **2012**, *287*, 82−97.

(11) Pitsch, F.; Krull, F. F.; Agel, F.; Schulz, P.; Wasserscheid, P.; Melin, T.; Wessling, M. An adaptive self-healing ionic liquid nanocomposite membrane for olefin-paraffin separations. *Adv. Mater.* **2012**, *24* (31), 4306−4310.

(12) Miranda, D. M. V. D.; Dutra, L. D. S.; Way, D.; Amaral, N.; Wegenast, F.; Scaldaferri, M. C.; Jesus, N.; Pinto, J. C. A bibliometric survey of paraffin/olefin separation using membranes. *Membranes* **2019**, *9* (12), 157 DOI: 10.3390/membranes9120157.

(13) Das, M.; Koros, W. J. Performance of 6FDA-6FpDA polyimide for propylene/propane separations. *J. Membr. Sci.* **2010**, *365* (1−2), 399−408.

(14) Krol, J. J.; Boerrigter, M.; Koops, G. H. Polyimide hollow fiber gas separation membranes: preparation and the suppression of plasticization in propane/propylene environments. *J. Membr. Sci.* **2001**, *184* (2), 275−286.

(15) Salleh, W. N. W.; Ismail, A. F.; Matsuura, T.; Abdullah, M. S. Precursor selection and process conditions in the preparation of carbon membrane for gas separation: A review. *Sep. Purif. Rev.* **2011**, *40* (4), 261−311.

(16) Swaidan, R.; Ma, X.; Litwiller, E.; Pinnau, I. High pressure pure- and mixed-gas separation of CO_2/CH_4 by thermally-rearranged and carbon molecular sieve membranes derived from a polyimide of intrinsic microporosity. *J. Membr. Sci.* **2013**, *447*, 387−394.

(17) Liang, J.; Wang, Z.; Huang, M.; Wu, S.; Shi, Y.; Zhang, Y.; Jin, J. Effects on carbon molecular sieve membrane properties for a precursor polyimide with simultaneous flatness and contortion in the repeat unit. *ChemSusChem* **2020**, *13* (20), 5531−5538.

(18) Richter, H.; Voss, H.; Kaltenborn, N.; Kaemnitz, S.; Wollbrink, A.; Feldhoff, A.; Caro, J.; Roitsch, S.; Voigt, I. High-flux carbon molecular sieve membranes for gas separation. *Angew. Chem., Int. Ed.* **2017**, *56* (27), 7760−7763.

(19) Saufi, S. M.; Ismail, A. F. Fabrication of carbon membranes for gas separation - a review. *Carbon* **2004**, *42* (2), 241−259.

(20) Qin, G.; Cao, X.; Wen, H.; Wei, W.; da Costa, J. C. D. Fine ultra-micropore control using the intrinsic viscosity of precursors for high performance carbon molecular sieve membranes. *Sep. Purif. Technol.* **2017**, *177*, 129−134.

(21) Rungta, M.; Wenz, G. B.; Zhang, C.; Xu, L.; Qiu, W.; Adams, J. S.; Koros, W. J. Carbon molecular sieve structure development and membrane performance relationships. *Carbon* **2017**, *115*, 237−248.

(22) Steel, K. M.; Koros, W. J. Investigation of porosity of carbon materials and related effects on gas separation properties. *Carbon* **2003**, *41* (2), 253−266.

(23) Kim, S. J.; Lee, P. S.; Chang, J. S.; Nam, S. E.; Park, Y. I. Preparation of carbon molecular sieve membranes on low-cost alumina hollow fibers for use in C_3H_6/C_3H_8 separation. *Sep. Purif. Technol.* **2018**, *194*, 443−450.

(24) Cui, L.; Qiu, W.; Paul, D. R.; Koros, W. J. Physical aging of 6FDA-based polyimide membranes monitored by gas permeability. *Polymer* **2011**, *52* (15), 3374−3380.

(25) Steel, K. M.; Koros, W. J. An investigation of the effects of pyrolysis parameters on gas separation properties of carbon materials. *Carbon* **2005**, *43* (9), 1843−1856.

(26) Liu, J.; Xiao, Y.; Chung, T. S. Flexible thermally treated 3D PIM-CD molecular sieve membranes exceeding the upper bound line for propylene/propane separation. *J. Mater. Chem. A* **2017**, *5* (9), 4583−4595.

(27) Swaidan, R. J.; Ma, X.; Pinnau, I. Spirobisindane-based polyimide as efficient precursor of thermally-rearranged and carbon molecular sieve membranes for enhanced propylene/propane separation. *J. Membr. Sci.* **2016**, *520*, 983−989.

(28) Shin, J. H.; Yu, H. J.; Park, J.; Lee, A. S.; Hwang, S. S.; Kim, S. J.; Park, S.; Cho, K. Y.; Won, W.; Lee, J. S. Fluorine-containing polyimide/polysilsesquioxane carbon molecular sieve membranes and techno-economic evaluation thereof for C_3H_6/C_3H_8 separation. *J. Membr. Sci.* **2020**, *598*, No. 117660.

(29) Salinas, O.; Ma, X.; Litwiller, E.; Pinnau, I. High-performance carbon molecular sieve membranes for ethylene/ethane separation derived from an intrinsically microporous polyimide. *J. Membr. Sci.* **2016**, *500*, 115−123.

(30) Lee, W. H.; Bae, J. Y.; Yushkin, A.; Efimov, M.; Jung, J. T.; Volkov, A.; Lee, Y. M. Energy and time efficient infrared (IR) irradiation treatment for preparing thermally rearranged (TR) and carbon molecular sieve (CMS) membranes for gas separation. *J. Membr. Sci.* **2020**, *613*, No. 118477.

(31) Teixeira, M.; Campo, M. C.; Tanaka, D. A. P.; Tanco, M. A. L.; Magen, C.; Mendes, A. Composite phenolic resin-based carbon

molecular sieve membranes for gas separation. *Carbon* **2011**, *49*, 4348−4358.
(32) Shi, Y.; Liang, J.; Shrestha, B. B.; Wang, Z.; Zhang, Y.; Jin, J. Enhancing the CO_2 plasticization resistance of thin polymeric membranes by designing metal-polymer complexes. *Sep. Purif. Technol.* **2022**, *289*, No. 120699.
(33) He, J. J.; Yang, H. X.; Zheng, F.; Yang, S. Y. Dielectric properties of fluorinated aromatic polyimide films with rigid polymer backbones. *Polymers* **2022**, *14* (3), 649.
(34) Kim, S. J.; Kwon, Y.; Kim, D.; Park, H.; Cho, Y. H.; Nam, S. E.; Park, Y. I. A review on polymer precursors of carbon molecular sieve membranes for olefin/paraffin separation. *Membranes* **2021**, *11*, 482.
(35) Arab, P.; Liu, Z.; Nasser, M.; Qiu, W.; Martinez, M.; Flick, D.; Roy, A.; Liu, J.; Koros, W. J. Subtle penetrant size effects on separation of carbon molecular sieve membranes derived from 6FDA:BPDA-DAM polyimide. *Carbon* **2021**, *184*, 214−222.
(36) Karunaweera, C.; Musselman, I. H.; Balkus, K. J., Jr.; Ferraris, J. P. Fabrication and characterization of aging resistant carbon molecular sieve membranes for C-3 separation using high molecular weight crosslinkable polyimide, 6FDA-DABA. *J. Membr. Sci.* **2019**, *581*, 430−438.
(37) Okamoto, K. I.; Kawamura, S.; Yoshino, M.; Kita, H.; Hirayama, Y.; Tanihara, N.; Kusuki, Y. Olefin/paraffin separation through carbonized membranes derived from an asymmetric polyimide hollow fiber membrane. *Ind. Eng. Chem. Res.* **1999**, *38* (11), 4424−4432.
(38) Yoshino, M.; Nakamura, S.; Kita, H.; Okamoto, K.; Tanihara, N.; Kusuki, Y. Olefin/paraffin separation performance of asymmetric hollow fiber membrane of 6FDA/BPDA-DDBT copolyimide. *J. Membr. Sci.* **2003**, *212* (1−2), 13−27.
(39) Islam, M. N.; Zhou, W. L.; Honda, T.; Tanaka, K.; Kita, H.; Okamoto, K. Preparation and gas separation performance of flexible pyrolytic membranes by low-temperature pyrolysis of sulfonated polyimides. *J. Membr. Sci.* **2005**, *261* (1−2), 17−26.

https://doi.org/10.1021/acs.iecr.3c02933
Ind. Eng. Chem. Res. 2023, 62, 18662−18671